# Oscillatory rarefied gas flow inside a three dimensional rectangular cavity

Peng Wang (王朋), Wei Su (苏微), and Yonghao Zhang (张勇豪)

Citation: Physics of Fluids **30**, 102002 (2018); doi: 10.1063/1.5052253
View online: https://doi.org/10.1063/1.5052253
View Table of Contents: http://aip.scitation.org/toc/phf/30/10
Published by the American Institute of Physics

# Oscillatory rarefied gas flow inside a three dimensional rectangular cavity

Peng Wang (王朋), Wei Su (苏微), and Yonghao Zhang (张勇豪)[a)]
*James Weir Fluids Laboratory, Department of Mechanical and Aerospace Engineering, University of Strathclyde, Glasgow G1 1XJ, United Kingdom*

(Received 15 August 2018; accepted 18 September 2018; published online 19 October 2018)

The oscillatory rarefied gas flow in a three-dimensional (3D) rectangular cavity, which is frequently encountered in micro-electro-mechanical systems, is investigated on the basis of the gas kinetic theory. The effects of the cavity aspect ratio, the cavity depth ratio, and the oscillation frequency of the driving lid on flow characteristics and damping force are systematically studied using the discrete unified gas-kinetic scheme over a broad range of gas rarefactions. For the highly rarefied flow, when the lid oscillates at a low frequency, as a consequence of the strong rarefaction effect, the damping force on the lid in a 3D cavity could even be smaller than that of a corresponding 2D one (i.e., the depth in the lateral direction approaching infinity). This finding contradicts our intuitive understanding that the damping force is expected to be amplified due to the presence of the lateral walls. Meanwhile, when the lid oscillation frequency becomes sufficiently high, due to the effect of gas anti-resonance, the damping force on the oscillating lid will increase again as the depth reduces for the highly rarefied flow. In addition, the gas resonance and anti-resonance found inside the 2D cavity also appear in 3D ones, and the anti-resonance and resonance frequencies as a function of the cavity aspect ratio are nearly the same. However, the presence of the lateral walls will suppress their formation: the smaller the depth, the weaker the intensity of the (anti-)resonance. These findings can help to design the structure of the micro-electro-mechanical devices. 
https://doi.org/10.1063/1.5052253

## I. INTRODUCTION

Oscillatory gas flows are frequently encountered in micro-electro-mechanical systems (MEMS),[1] including the inertial sensors and resonators, the actuators, and the micro-accelerometers. With the miniaturization of the device structure, the characteristic dimension is reduced to the micro- and nano-scales, in which the surface-area-to-volume ratio is large and the gas flow is generally rarefied. Therefore, surface effects such as the damping force exerted on the oscillating parts by the rarefied gas should be carefully considered in the design of micro-devices with moving parts.[2]

When the mean free path (or collision frequency) of gas molecules is comparable or even larger (smaller) than the characteristic flow length (oscillation frequency), the traditional Navier-Stokes equations fail, due to the gas rarefaction, which not only causes velocity slip and temperature jump at solid surfaces, but also invalidates the linear constitutive relations for stress and heat flux. The degree of gas rarefaction is normally characterized by the Knudsen number, defined as the ratio of the gas mean free path to the characteristic length. Alternatively, it can also be defined as the ratio of the oscillation frequency and the collision frequency of gas molecules. Due to micro-/nano-scale dimension of MEMS devices, most of them operate in the slip ($10^{-3} \lesssim \mathrm{Kn} \lesssim 0.1$) and early transition regimes ($0.1 \lesssim \mathrm{Kn} \lesssim 1$).[3,4] Instead of the Navier-Stokes equations, the gas kinetic model should be adopted for rarefied flow analysis.[5,6]

To date, gas damping in MEMS devices has been investigated using the Boltzmann equation and its kinetic model equations.[6] Specifically, the one-dimensional (1D) oscillatory flow has been extensively studied over a wide range of Knudsen numbers, where analytical solutions are obtained in the limit of near continuum regime ($\mathrm{Kn} \lesssim 0.1$)[3,7] and free molecular regime ($\mathrm{Kn} \gtrsim 10$),[5,7,8] while in the transition regime ($0.1 \lesssim \mathrm{Kn} \lesssim 10$), the problem is numerically solved using the direct simulation Monte Carlo (DSMC) method[3,8–13] and the discrete velocity method (DVM).[4,5,7,14–18] For multi-dimensional flows such as the oscillatory gas flow inside a two-dimensional (2D) cavity,[17,19,20] it is difficult to derive the analytical solution; thus, the flow in all the regimes needs to be solved numerically. However, the DSMC method and DVM are computationally expensive for flows near the hydrodynamic regime.[21] This is due to the well-known intrinsic limitation that the computational time step and spatial mesh size are required to be smaller than the local mean collision time and the mean free path of gas molecules, respectively, if the free streaming and collisions of gas molecules are dealt with separately.[22] Particularly, the DSMC is too costly for low-speed flows typically found in MEMS devices. As a result, previous investigations on the oscillatory rarefied gas flows have mainly been restricted in the transition and free molecular regimes. In addition, despite the three dimensional (3D) nature of flow in the MEMS devices, a number of simplified

[a)]yonghao.zhang@strath.ac.uk

 

analytical models have often been used to evaluate damping which are typically based on the 1D Couette flow or Stokes flow.[23] For an optimal design of oscillatory MEMS devices, we need an improved understanding of gas dynamics and its effect on damping, which is the main motivation of this study.

In this work, for the first time, the oscillatory rarefied but low-speed gas flow inside a 3D rectangular cavity is investigated on the basis of the Bhatnagar-Gross-Krook (BGK) equation.[24] In addition to gas rarefaction, the influences on gas dynamics and damping force from various oscillation frequencies, aspect ratios, and depth ratios in the lateral direction of a 3D cavity are investigated using the discrete unified gas-kinetic scheme (DUGKS) that handles the streaming and collision simultaneously.[25,26] The remainder of the paper is organized as follows. We introduce the formulation of the problem as well as the gas-kinetic BGK equation in Sec. II. Computational details are described in Sec. III. The numerical results of the flow field and damping force are presented, compared, and discussed in Sec. IV, which is followed by the conclusions in Sec. V.

## II. PROBLEM FORMULATION

We consider a rarefied gas flow in a 3D rectangular cavity driven by a lid at $y = |OH| = \mathcal{H}$, where $O$ is the origin of the coordinate, as illustrated in Fig. 1. The lid oscillates harmonically in the $z$-direction with a frequency $\omega$. The time-varying velocity of the oscillating lid $U_z$ is given as

$$U_z(t) = W_0 \cos(\omega t), \tag{1}$$

where $W_0$ is the amplitude of the oscillating velocity and $t$ is the time. The other walls at $x = 0$, $x = |OD| = \mathcal{D}$, $z = 0$, $z = |OA| = \mathcal{A}$, and $y = 0$ are fixed, and all the walls are isothermal with a temperature $T_w$.

The problem considered is characterized by the cavity aspect ratio $A_r$, the cavity depth ratio $D_r$, the Strouhal number St, and the Knudsen number Kn, which are, respectively, defined as

$$A_r = \frac{\mathcal{A}}{\mathcal{H}}, \quad D_r = \frac{\mathcal{D}}{\mathcal{H}}, \quad \mathrm{St} = \frac{\omega \mathcal{H}}{v_m}, \quad \mathrm{Kn} = \frac{\lambda}{\mathcal{H}}, \tag{2}$$

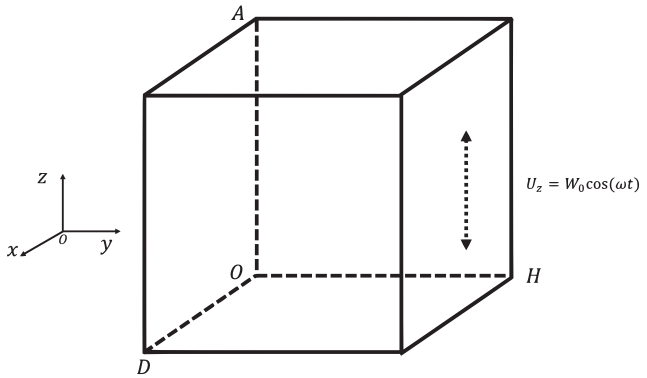


FIG. 1. Schematic of the oscillatory flow in a 3D rectangular cavity, where $O$ is the origin of the coordinate.

where $v_m = \sqrt{2RT_w}$ is the most probable molecular velocity with $R$ being the specific gas constant. The molecular mean free path $\lambda$ is related to the gas shear viscosity $\mu$ as

$$\lambda = \frac{\mu(T = T_w)}{p}\sqrt{\frac{\pi RT_w}{2}}, \tag{3}$$

where $p = \rho RT_w$ is the pressure and $\rho$ is the density. Note that the amplitude of the oscillating velocity satisfies $W_0 \ll v_m$ so that the temperature perturbation is sufficiently small and the flow inside the cavity can be considered as being isothermal. The BGK equation is therefore adopted to describe the flow response. In the absence of external force, it takes the form of[24]

$$\frac{\partial f}{\partial t} + \boldsymbol{\xi} \cdot \nabla f = -\frac{1}{\tau}[f - f^{eq}], \tag{4}$$

where $f(\boldsymbol{x}, \boldsymbol{\xi}, t)$ is the velocity distribution function of gas molecules at the position $\boldsymbol{x} = (x, y, z)$ and the time $t$, with $\boldsymbol{\xi} = (\xi_x, \xi_y, \xi_z)$ being the molecular velocity. The collision time $\tau$ in Eq. (4) is evaluated from the viscosity $\mu$ and the pressure by $\tau = \mu/p$. The Maxwellian equilibrium distribution function $f^{eq}$ is given as

$$f^{eq} = \frac{\rho}{(2\pi RT)^{3/2}} \exp\left(-\frac{c^2}{2RT}\right), \tag{5}$$

where $\boldsymbol{c} = \boldsymbol{\xi} - \boldsymbol{U}$ is the peculiar velocity and $\boldsymbol{U} = \left(U_x, U_y, U_z\right)$ is the macroscopic flow velocity. The conservative variables $\boldsymbol{W} \equiv (\rho, \rho\boldsymbol{U}, \rho E)^T$ are calculated from the velocity moments of the velocity distribution function, $\boldsymbol{W} = \int \boldsymbol{\psi} f \mathrm{d}\boldsymbol{\xi}$, where $\boldsymbol{\psi} = \left(1, \boldsymbol{\xi}, \frac{1}{2}\xi^2\right)^T$. Note that for an ideal gas, the temperature is related to the total energy as $\rho E = \frac{1}{2}\rho U^2 + \frac{3}{2}\rho RT$.

The damping force, which is the amplitude of average shear stress acting on the oscillating lid, is an important parameter in the design of MEMS devices. In this work, the average shear stress exerted on the oscillating lid is defined as

$$\bar{P}_{yz}(y = \mathcal{H}) = \frac{1}{\mathcal{A}}\int_0^{\mathcal{A}} P_{yz}(y = \mathcal{H}, z)dz, \tag{6}$$

where $P_{yz}$ is the depth-average shear stress,

$$P_{yz}(y = \mathcal{H}, z) = \frac{1}{\mathcal{D}}\int_0^{\mathcal{D}} \mathcal{P}_{yz}(x, y = \mathcal{H}, z)dx, \tag{7}$$

with the shear stress $\mathcal{P}_{yz}$ being calculated as

$$\mathcal{P}_{yz} = \int (\xi_y - U_y)(\xi_z - U_z) f d\xi_x d\xi_y d\xi_z. \tag{8}$$

Note that the component of average shear stress along the $x$-axis on the oscillating lid, which is about one order of magnitude smaller than $\bar{P}_{yz}(y = \mathcal{H})$, is neglected in this study.

## III. NUMERICAL METHOD

The DUGKS is used to solve the BGK equation,[25] which has been successfully applied to study the linear and nonlinear oscillatory gas flows inside a 2D rectangular cavity[20] covering all the flow regimes. The details of the DUGKS for the BGK model can be found in Guo *et al.*[25]

In order to accurately approximate the moments of velocity distribution function, the continuous molecular velocity

space $\left(\xi_x,\ \xi_y,\ \xi_z \in (-\infty, +\infty)\right)$ should be properly discretized according to the degree of gas rarefaction. The discretization is associated with a certain quadrature rule to compute the velocity integrals. In the present simulations, the Gauss-Hermit quadratures with 8 points and 16 points are applied in each velocity direction for Kn = 0.01 and Kn = 0.1, respectively, while the continuous molecular velocity space is truncated within $[-4\sqrt{2RT_w}, 4\sqrt{2RT_w}]$ and discretized by the trapezoidal rule with 32 non-uniform grid points in each velocity direction when Kn = 1.[27,28] In terms of the spatial discretization, a set of non-uniform meshes with $N_x \times N_y \times N_z$ grid points are adopted in the $x$, $y$, and $z$ directions, respectively, and the mesh resolution is gradually refined from the cavity center to the wall boundaries. The location of each control volume center $(x_i, y_j, z_k)$ is generated by $x_i = (\zeta_i + \zeta_{i+1})/2$, $y_j = (\zeta_j + \zeta_{j+1})/2$, $z_k = (\zeta_k + \zeta_{k+1})/2$, $0 \le i < N_x$, $0 \le j < N_y$, $0 \le k < N_z$, where $\zeta_i$ is defined as

$$\zeta_i = \frac{1}{2} + \frac{\tanh[a(i/N - 0.5)]}{\tanh(a/2)}, \quad i = 0, 1, 2, \ldots, N_{x,y,z} - 1. \tag{9}$$

Note that the constant $a$ determines the mesh distribution: the larger the $a$, the smaller the mesh size near the walls. Here $a$ in the $x$, $y$, and $z$ directions is set to be 2.5, 3.5, and 3.5, respectively. In all the numerical simulations, the height of the cavity is fixed at $\mathcal{H} = 1$. 48 points for Kn = 0.01, and 36 points for Kn = 0.1 and 1 are used per unit length in each direction. Independence of the results on the discretizations of the molecular velocity space and spatial space has been confirmed for these given conditions. Note that the results for Kn > 1 will not be presented here as they are very close to the results of Kn = 1, which is similarly reported in our previous work on a 2D cavity.[17,20]

The computational time step in the DUGKS is solely determined by the Courant-Friedrichs-Lewy (CFL) condition,[25] $\Delta t = \eta \Delta x_{min}/\xi_{max}$, where $\eta$ is the CFL number, $\Delta x_{min}$ is the minimum mesh size, and $\xi_{max}$ is the maximum discrete molecular speed. Note that the DUGKS has distinguished performance in robustness.[29] For instance, when Kn = 0.1, St = 2, $A_r = 1$, and $D_r = 1$, the change in the amplitude of average shear stress (6) on the oscillating lid is less than 0.05% when the CFL number varies from 0.01 to 0.8. Therefore, a relatively large CFL number can be used to reduce the computational time. In all the simulations, the CFL number $\eta \approx 0.5$ is set to satisfy $n\Delta t = \pi$, $n \in \mathbb{Z}^+$.

The model accuracy of the DUGKS has been exhaustively demonstrated.[21,29,30] In particular, the DUGKS for the oscillatory rarefied flow has been successfully used in our previous study,[20] where the results were validated by the solution of the Boltzmann equation using fast spectral method.[17] In addition, the DUGKS simulation of the 3D lid-driven rarefied cavity flow has also been verified by the DSMC data.[31] It is worthy to emphasize that the primary reason for adopting the DUGKS is that different from the traditional DVM, the grid size in the DUGKS is not necessary to be smaller than the mean free path in the near hydrodynamic regime, which allows the DUGKS to use much fewer grid points than the traditional DVM in describing the slip and continuum flows.[21,32,33] For example, when Kn = 0.01, $A_r = 1$, and $D_r = 1$, for St = 0, 2, and 20, with 48 mesh points per unit height, the maximum change in the amplitude of average shear stress on the oscillating lid is less than 0.2%, when compared to the results of 96 mesh points. With 48 grid points, the average mesh size is about twice of the mean free path of gas molecules.

## IV. RESULTS AND DISCUSSION

Numerical simulations covering a wide range of the Knudsen numbers, the Strouhal numbers, and the aspect and depth ratios of the cavity are performed by the DUGKS, with the diffuse boundary condition for gas-wall interactions.[20] Note that when the depth ratio $D_r$ approaches infinity, the 3D cavity is degenerated to 2D ones. Therefore, in this study, the effect of the cavity depth in the lateral direction is of particular interest, and the results on the corresponding 2D cavity are also included to show the 3D effect.

### A. Flow characteristics

The flow characteristics inside the cavity is investigated under two typical Knudsen numbers of Kn = 0.1 and 1 and two typical Strouhal numbers of St = 1 and 3. We are only interested in the results that have already reached the periodic "steady-state," that is, the solution at the next oscillation period will be exactly the same as the previous one. The results for the steady lid-driven cavity flow, i.e., St = 0, are also included for comparison. The dimension of the cavity is set as $A_r = D_r = 1$ unless otherwise stated. Since the velocity amplitude of the oscillation is far smaller than the sound speed, the flow field inside the cavity is symmetrical along the cross sections of $x = 0.5\mathcal{D}$ and $z = 0.5\mathcal{A}$. Therefore, flow properties in one-quarter ($\left[0, \frac{\mathcal{D}}{2}\right] \times [0, \mathcal{H}] \times \left[0, \frac{\mathcal{A}}{2}\right]$) of the cavity are taken into account. Note that the $x$-component velocity $U_x$ is not provided here as its value is about one order of magnitude smaller than the other two components.

Figure 2 shows the $z$-component velocity $U_z$ inside one-quarter of the cavity, while $U_z$ in the rest of the cavity can be obtained as

$$\begin{gathered} U_z(x, y, z) = U_z(\mathcal{D} - x, y, z), \\ x \times y \times z \in [\frac{\mathcal{D}}{2}, \mathcal{D}] \times [0, \mathcal{H}] \times [0, \frac{\mathcal{A}}{2}], \end{gathered} \tag{10a}$$

$$\begin{gathered} U_z(x, y, z) = U_z(\mathcal{D} - x, y, \mathcal{A} - z), \\ x \times y \times z \in [\frac{\mathcal{D}}{2}, \mathcal{D}] \times [0, \mathcal{H}] \times [\frac{\mathcal{A}}{2}, \mathcal{A}], \end{gathered} \tag{10b}$$

$$\begin{gathered} U_z(x, y, z) = U_z(x, y, \mathcal{A} - z), \\ x \times y \times z \in [0, \frac{\mathcal{D}}{2}] \times [0, \mathcal{H}] \times [\frac{\mathcal{A}}{2}, \mathcal{A}]. \end{gathered} \tag{10c}$$

Strong movement of the flow can mainly be seen near the oscillating plane; specifically, the maximum $U_z$ occurs in the center of the oscillating plate. Bearing in mind that when $D_r \to \infty$, the contourlines on the cross sections perpendicular to the $y$-axis should be a set of lines parallel to the $x$-axis. As the depth ratio decreases, the role of the lateral wall will be enhanced. As a result, when a finite depth ratio (e.g., $D_r = 1$) is applied, $U_z$ on the oscillating lid gradually decreases from the center to the lateral boundary,

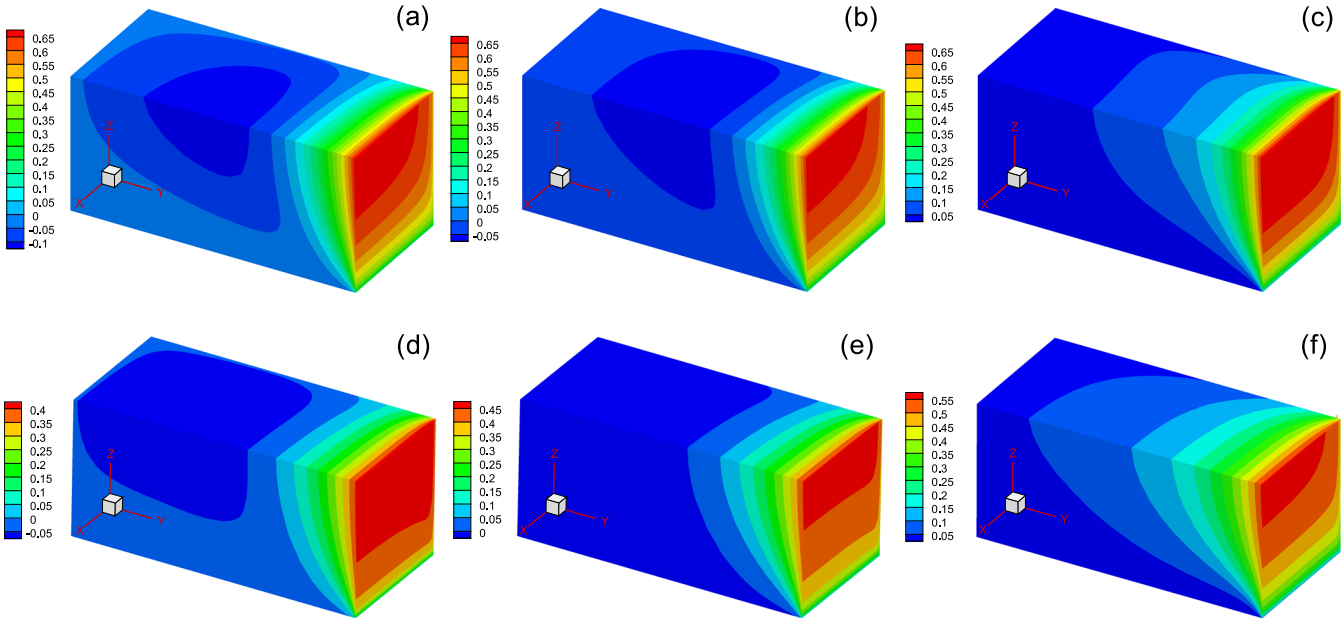


FIG. 2. Contours of the flow velocity $U_z$ when Kn = 0.1 (top row) and Kn = 1 (bottom row), with St = 0, 1, and 3 (from left to right column). Here $A_r = D_r = 1$ and $\omega t/2\pi = 0$. Note that due to symmetry, only one-quarter of the cavity is shown.

due to the friction from the lateral wall of $x = 0$; see Fig. 2. In addition, contourlines of $U_z$ on the oscillating lid for Kn = 1 is more flattened than those of Kn = 0.1, due to the weaker resistance from the walls for a larger Kn. That is to say, the effect of 3D structure is more visible for a smaller Kn. The velocity $U_z$ on the oscillating lid for Kn = 0.1 is larger than that of Kn = 1, because of the smaller slip velocity (difference between the wall speed and the gas flow velocity) for a smaller Kn.

The velocity $U_y$, which is perpendicular to the oscillating lid, is presented in Fig. 3. Similarly, for the other three parts of the cavity, $U_y$ can be computed as

$$U_y(x,y,z) = U_y(\mathcal{D}-x,y,z), \quad x\times y\times z \in [\frac{\mathcal{D}}{2},\mathcal{D}]\times[0,\mathcal{H}]\times[0,\frac{\mathcal{A}}{2}], \tag{11a}$$

$$U_y(x,y,z) = -U_y(\mathcal{D}-x,y,\mathcal{A}-z), \quad x\times y\times z \in [\frac{\mathcal{D}}{2},\mathcal{D}]\times[0,\mathcal{H}]\times[\frac{\mathcal{A}}{2},\mathcal{A}], \tag{11b}$$

$$U_y(x,y,z) = -U_y(x,y,\mathcal{A}-z), \quad x\times y\times z \in [0,\frac{\mathcal{D}}{2}]\times[0,\mathcal{H}]\times[\frac{\mathcal{A}}{2},\mathcal{A}]. \tag{11c}$$

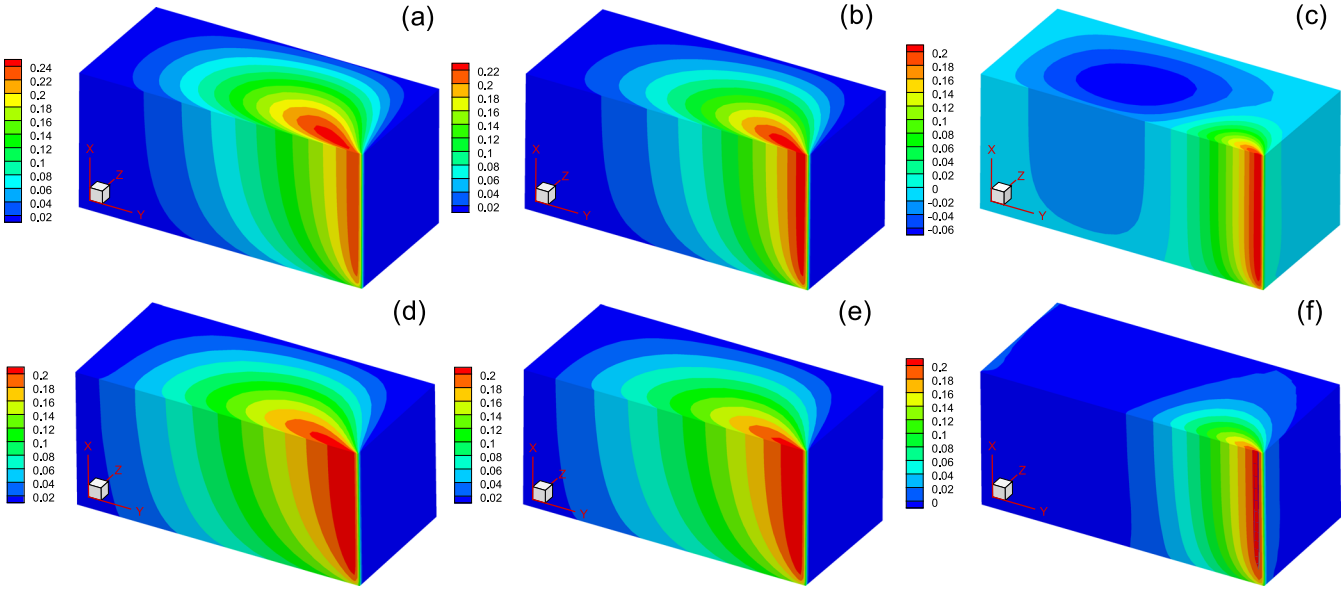


FIG. 3. Contours of the flow velocity $U_y$ in one-quarter of the cavity when Kn = 0.1 (top row) and Kn = 1 (bottom row), with St = 0, 1, and 3 (from left to right column). Here $A_r = D_r = 1$, and $\omega t/2\pi = 0$.

For all the Strouhal numbers, the maximum $U_y$ emerges at the joint corner of planes at $y = \mathcal{H}$ and $z = 0$. As St increases, the region in which the gas flow is disturbed by the moving lid is squeezed toward the joint corner, and when Kn = 0.1 and St = 3, the negative $U_y$ appears. In addition, due to the presence of lateral walls, $U_y$ is decreased from the bulk region to the boundaries along the $x$ axis. Finally, as expected, the variation of $U_y$ inside the cavity is much smaller than that of $U_z$.

Figure 4 shows the evolution of gas flow velocity magnitude ($\sqrt{U_x^2 + U_y^2 + U_z^2}$) inside one-quarter of the cavity during the first half oscillation period for Kn = 0.1 and St = 3, with $A_r = D_r = 1$. The distribution of the velocity magnitude in the next half period is the same. When $\omega t = 0$ and $U_z = W_0$, the maximum velocity magnitude is located near the oscillating lid; see Fig. 4(a). As the velocity of the lid is reduced to $\sqrt{2}W_0/2$ at $\omega t = 0.25\pi$, the perturbation from the oscillating lid has penetrated into the deep cavity. When $U_z = 0$ at $\omega t = 0.5\pi$, the flow velocity at the oscillating lid falls back to zero, but the maximum magnitude appears away from the driven lid. When the oscillating velocity is $U_z = -\sqrt{2}W_0/2$ at $\omega t = 0.75\pi$, the intense movement is back to the oscillating lid. Nevertheless, the strong flow motion always occurs near the oscillating plane during the whole period.

## B. Damping force on the oscillating plane

### 1. The shear stress on the oscillating plane

The shear stress $\mathcal{P}_{yz}$ exerted on the oscillating lid as calculated by Eq. (8) is depicted in Fig. 5, where $A_r = 1$, $D_r = 1$, and $\omega t/2\pi = 0$. The results are similar for other aspect and depth ratios. In the limit of the depth ratio approaching infinity, the flow pattern inside the cavity is approximately two dimensional; hence, the contourlines should be parallel to the $x$-axis. For a finite depth ratio, however, due to the presence of the lateral walls, $|\mathcal{P}_{yz}|$ is expected to be enhanced. It is the case for Kn = 0.1 with St = 1 and 3, as shown in Figs. 5(a) and 5(b), respectively, where $|\mathcal{P}_{yz}|$ is increased from the bulk region to the lateral walls along the $x$-axis. However, for Kn = 1, the situation is reversed: when St = 1 [see Fig. 5(c)], $|\mathcal{P}_{yz}|$ declines from the bulk region to the lateral wall. Interestingly, when St increases to 3, the $|\mathcal{P}_{yz}|$ becomes larger again toward the lateral wall [see Fig. 5(d)], which is the same as the case of Kn = 0.1. The reason responsible to this intriguing phenomenon will be discussed in detail in the Sec. IV B 3. In addition, the variation of $\mathcal{P}_{yz}$ on the oscillating lid when Kn = 0.1 is about three times of that for Kn = 1.

### 2. The depth average shear stress

The absolute value of depth-average shear stress $|P_{yz}|$ on the oscillating plane along the $z$-axis is shown in Fig. 6 for

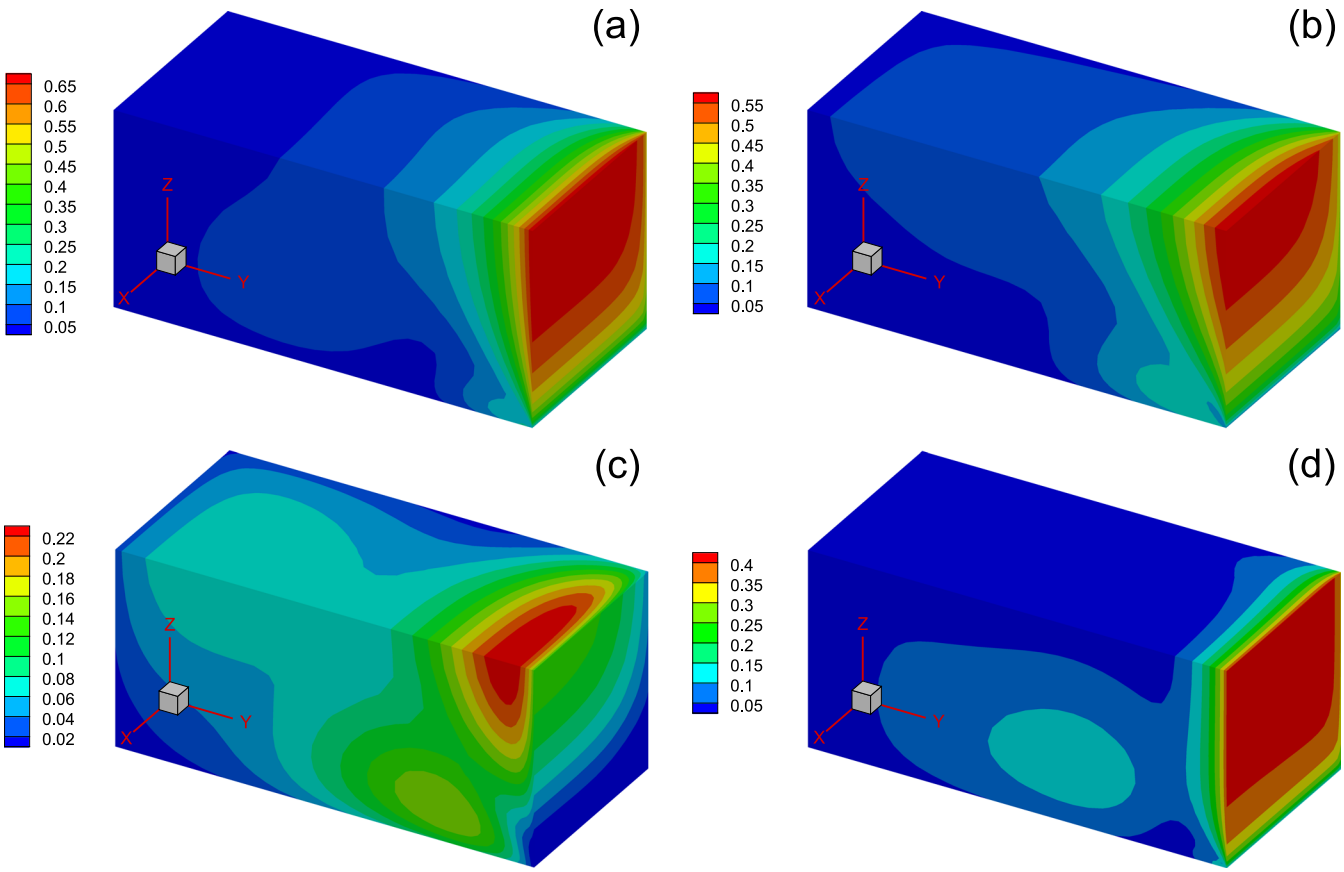


FIG. 4. Evolution of the velocity magnitude in one-quarter of the cavity for Kn = 0.1, St = 3, and $A_r = D_r = 1$: (a) $\omega t = 0$; (b) $\omega t = 0.25\pi$; (c) $\omega t = 0.5\pi$; and (d) $\omega t = 0.75\pi$.

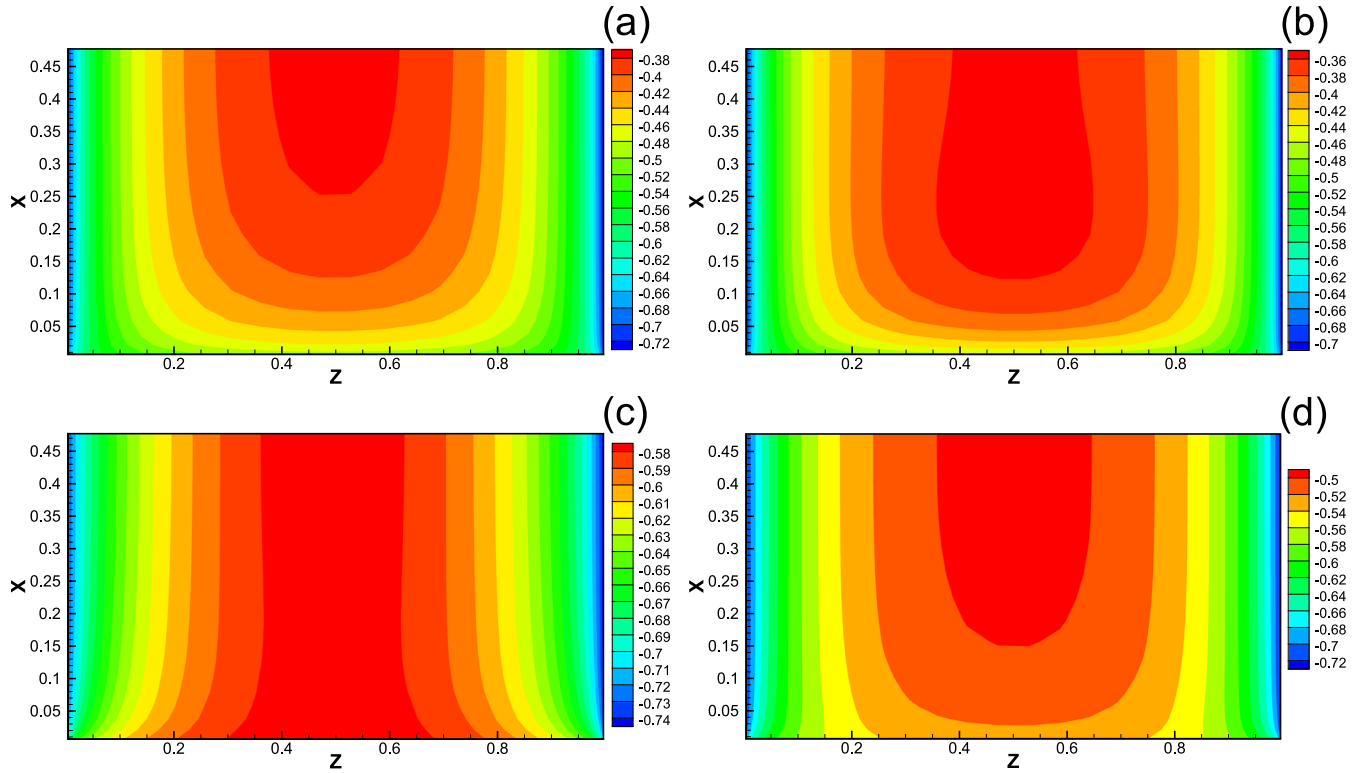


FIG. 5. Contour of the shear stress $\mathcal{P}_{yz}$ on the oscillating plane $y = \mathcal{H}$ for (a) Kn = 0.1, St = 1; (b) Kn = 0.1, St = 3; (c) Kn = 1, St = 1; and (d) Kn = 1, St = 3, where $A_r = D_r = 1$ and $\omega t/2\pi = 0$. The half of plane $y = \mathcal{H}$ is presented due to the symmetry along the cross section $x = 0.5$.

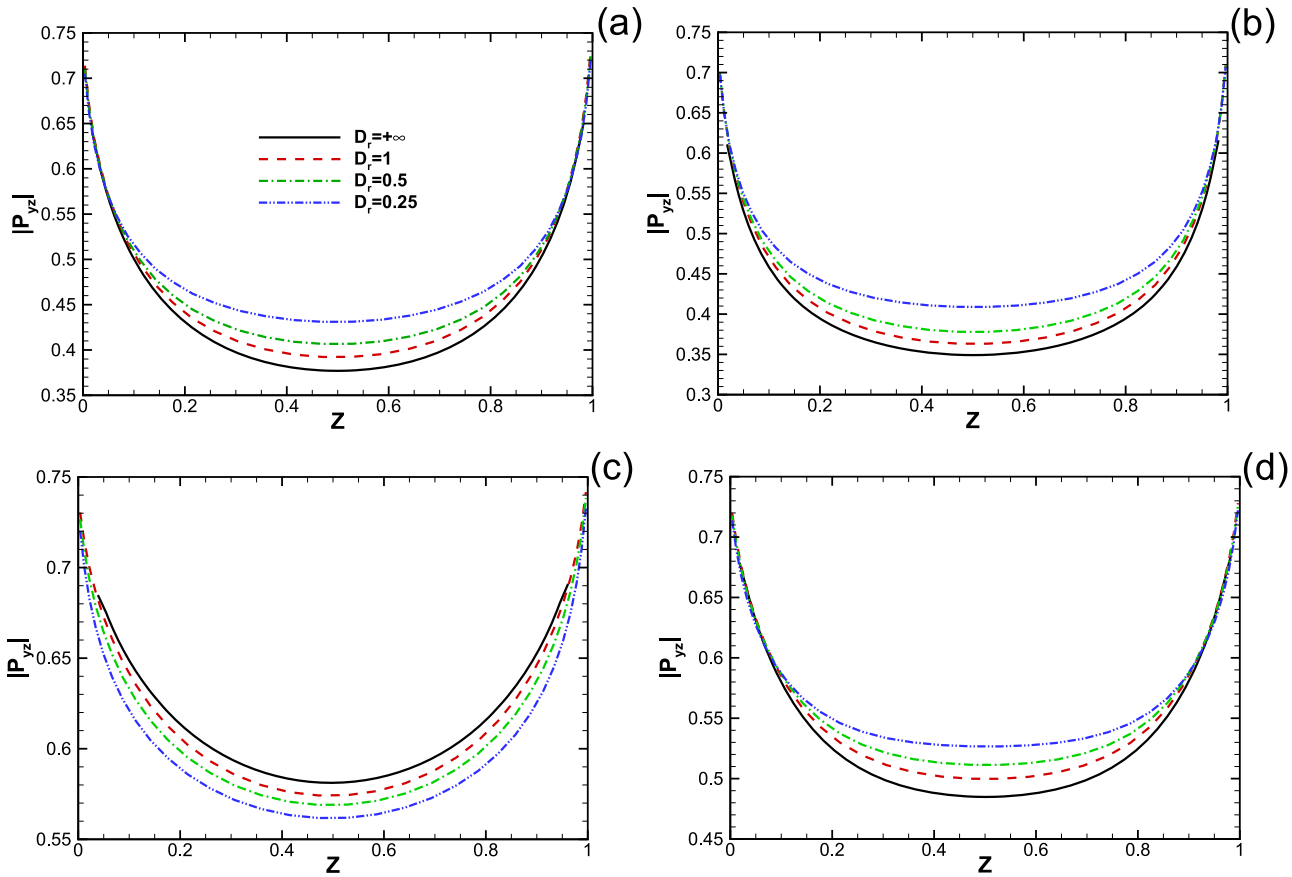


FIG. 6. The absolute value of the depth-average shear stress $|P_{yz}|$, as defined in Eq. (7), on the oscillating lid when (a) Kn = 0.1, St = 1; (b) Kn = 0.1, St = 3; (c) Kn = 1, St = 1; and (d) Kn = 1, St = 3, with different $D_r$. Here $A_r = 1$ and $\omega t/2\pi = 0$.

$A_r = 1$ with different $D_r$. The results for $D_r = \infty$, at which the 3D cavity degenerates to 2D, are also included for comparison. At both the side walls, $|P_{yz}|$ reaches the maximum and then reduces to the minimum in the middle of the cavity along the $z$-axis. As the depth ratio increases, $|P_{yz}|$ decreases and eventually approaches the value when $D_r = \infty$. However, this is not the case for Kn = 1 and St = 1 [see Fig. 6(c)], where $|P_{yz}|$ increases with the depth ratio. This is a consequence of the two competing effects of Kn and St on $|P_{yz}|$, as shown in Fig. 5.

### 3. The damping force on the oscillating plane

In this section, we consider the damping force, i.e., the amplitude of average shear stress on the oscillating plane. First, we try to analyze the behavior of damping force in the limit of $\omega \to \infty$. In this case, binary collisions of gas molecules are negligible[7] because the oscillation frequency $\omega$ is much larger than the mean collision frequency. As a consequence, Eq. (4) is degenerated to the collisionless Boltzmann equation,

$$\frac{\partial f}{\partial t} + \xi_x \frac{\partial f}{\partial x} + \xi_y \frac{\partial f}{\partial y} + \xi_z \frac{\partial f}{\partial z} = 0. \tag{12}$$

In addition, due to small amplitude of the oscillating velocity, all the flow properties oscillate around their equilibrium values with the same frequency $\omega$ as the oscillation lid. Thus, the velocity distribution function can be expressed as

$$f(x, y, z, t, \boldsymbol{\xi}) = f^{eq} + \Re\left[\exp(i\omega t) f'(x, y, z, \boldsymbol{\xi})\right] W_0, \tag{13}$$

where the equation for $f'$ is independent of time,

$$i\mathrm{St} f' + \xi_x \frac{\partial f'}{\partial x} + \xi_y \frac{\partial f'}{\partial y} + \xi_z \frac{\partial f'}{\partial z} = 0. \tag{14}$$

Integrating (14) with respect to $x$ and $z$ on the oscillating plane, one can obtain

$$i\mathrm{St} g + \xi_y \frac{\partial g}{\partial y} = \xi_x \frac{f'(x=0) - f'(x=\mathcal{D})}{\mathcal{D}} + \xi_z \frac{f'(z=0) - f'(x=\mathcal{A})}{\mathcal{A}}, \tag{15}$$

where $g = \int_0^{\mathcal{D}} \int_0^{\mathcal{A}} f' dx dz / \mathcal{D}\mathcal{A}$ is the average velocity distribution function. As stated above, for this linear oscillation, the distribution functions on the oscillating plane are symmetric along the centerlines so that the right-hand side of (15) can be neglected. Hence together with the diffuse boundary condition,[20] the analytical solution of the amplitude of average shear stress on the oscillating lid can be easily obtained,[17] which is equal to $1/\sqrt{\pi} \approx 0.564$. From this analysis, we can also learn that the amplitude of average shear stress in the high oscillating frequency limit is independent of the aspect and depth ratios of the cavity, which will be numerically verified below.

Figure 7 depicts the damping force $|\bar{P}_{yz}|$ on the oscillating lid as a function of the Strouhal number, where the depth ratio $D_r = 0.5$. The results are presented at three typical Knudsen numbers, i.e., Kn = 0.01, 0.1, and 1. It is observed that the change in $|\bar{P}_{yz}|$ with respect to St for a finite depth ratio possesses a similar behavior to that when $D_r = \infty$.[17,20] First, $|\bar{P}_{yz}|$ on the oscillating lid increases as the aspect ratio $A_r$ becomes smaller. Second, $|\bar{P}_{yz}|$ changes non-monotonically with respect to St. Finally, the variation of $|\bar{P}_{yz}|$ for Kn = 0.01 is more complicated than those at larger Knudsen numbers. When Kn = 0.01, $|\bar{P}_{yz}|$ will not approach the limit of $1/\sqrt{\pi}$ but increases with St at moderately high frequencies (St < 50).

However, the lateral walls could have a manifest impact on the damping force exerted on the oscillating plate. Figure 8 shows $|\bar{P}_{yz}|$ as a function of St for two typical Knudsen numbers, Kn = 0.1 and 1, with different values of $D_r$. When Kn = 0.1 and $D_r = 0.25$, as St increases, $|\bar{P}_{yz}|$ first declines to a local minimum at St ≈ 2.5 and then grows toward the limiting value of $1/\sqrt{\pi}$ at the high frequency; see Fig. 8(a). However, when $D_r = \infty$, an additional local maximum $|\bar{P}_{yz}|$ emerges at $St \approx 1$.[17,20] As the depth ratio is decreased to $D_r = 0.5$, such a local peak disappears. That is to say, the presence of lateral walls could suppress the formation of the local maximum of $|\bar{P}_{yz}|$. On the other hand, we note that the value of the minimum damping force increases with decreasing $D_r$.

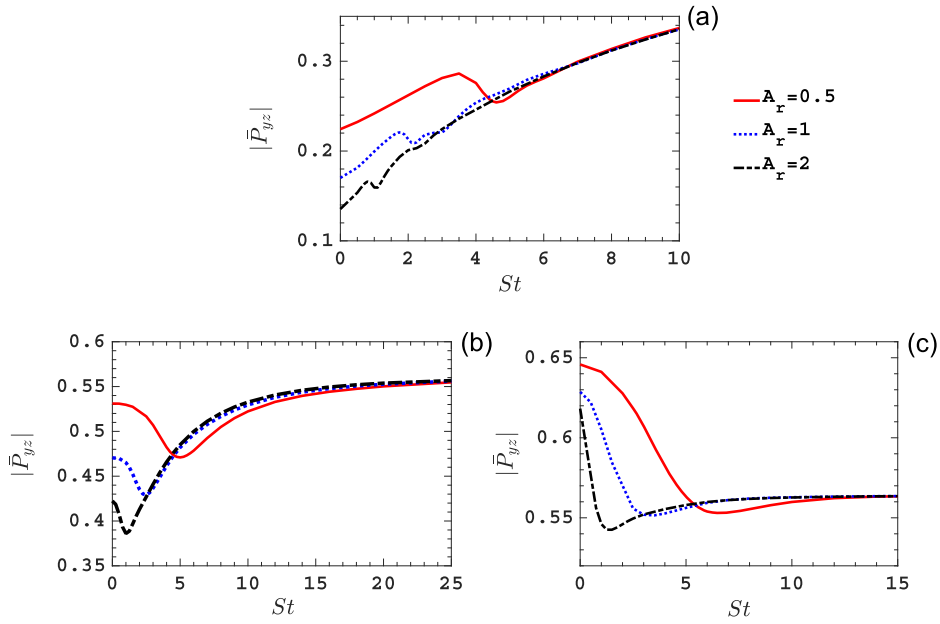


FIG. 7. The amplitude of average shear stress on the oscillating lid as a function of St for (a) Kn = 0.01, (b) Kn = 0.1, and (c) Kn = 1, with $D_r = 0.5$ and $A_r = 0.5$, 1, and 2.

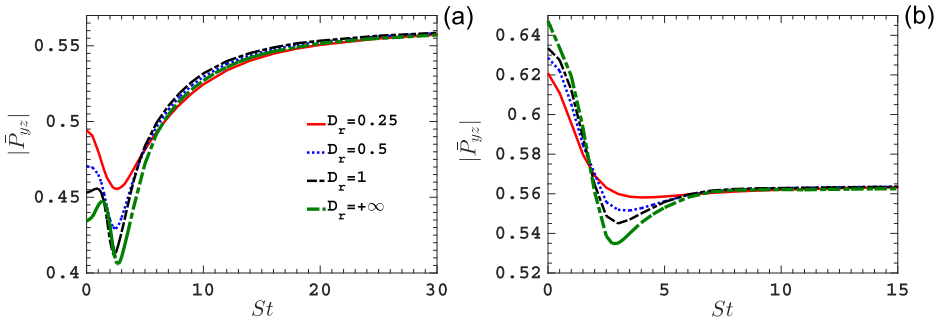


FIG. 8. The amplitude of average shear stress on the oscillating lid as a function of St for (a) Kn = 0.1 and (b) Kn = 1, with $A_r = 1$ and $D_r = 0.25, 0.5, 1,$ and $\infty$.

In fact, the local maximum and minimum of $|\bar{P}_{yz}|$ are due to the gas resonance and anti-resonance, respectively, which will be discussed later. From Fig. 8, we can also find that irrespective of the depth ratio, all $|\bar{P}_{yz}|$ approach the limit of $1/\sqrt{\pi}$ when the oscillation frequency is sufficiently high, which agrees well with the above theoretical analysis. In addition, the depth ratio seems to have limited effect on the critical Strouhal number (at which the local minimum occurs), which will be theoretically analyzed in Subsection IV C.

Furthermore, when Kn = 0.1, as $D_r$ increases, $|\bar{P}_{yz}|$ generally declines toward the value in the limit of $D_r = \infty$. For Kn = 1 and St $\lesssim 2$, however, the situation is reversed: an increase in $D_r$ enlarges $|\bar{P}_{yz}|$ on the oscillating lid, which contradicts the intuitive understanding that the presence of the lateral walls is expected to increase the damping force on the oscillating lid. For St $\gtrsim 2$, an increase in $D_r$ will again lead to a reduction in $|\bar{P}_{yz}|$ on the oscillating lid. These observations are consistent with the findings presented in Figs. 6(c) and 6(d) for Kn = 1 with St = 1 and St = 3, respectively. Note that the results of Kn < 0.1 and Kn > 1 are similar to those of Kn = 0.1 and Kn = 1, respectively.

We can explain these as follows. We first consider the case of St = 0. It is well-recognized that the shear stress is produced from the cumulation of the hydrodynamic and the rarefied effects. When the Knudsen number is sufficiently small, e.g., Kn $\ll 1$, the intermolecular collisions are rather frequent so that the hydrodynamic part is dominant and the shear stress satisfies the Newton's constitutive law; that is to say, the value of shear stress on the oscillating lid is merely determined by the difference of the velocities between the oscillating lid and the flow fluid at the oscillating lid, which is expected to be enlarged due to the presence of the lateral walls. Therefore, for the near continuum flows, the shear stress should increase with decreasing the depth ratio. On the other hand, when Kn $\gg 1$, binary collisions of the molecules can be neglected such that the shear stress on the oscillating lid is mainly determined by the direct collision of the gas molecules with the lid surface per unit time. The presence of the lateral walls could interrupt the travel path of gas molecules, which will therefore reduce the probability of gas molecules colliding with the oscillating lid. Consequently, for the highly rarefied flows, the shear stress on the oscillating lid is expected to decrease with the reduction in the depth ratio. However, as the oscillation frequency increases, the gas anti-resonance emerges, which will increase the damping force on the lid with the reduction in the depth ratio.

### C. Scaling law for resonance and anti-resonance frequencies and aspect ratio

The local drop and rise of the damping force in Figs. 7 and 8 can be interpreted qualitatively by the theory of gas anti-resonance and resonance, respectively. For the free molecular flow, the molecules leaving the oscillating lid $y = \mathcal{H}$ with the most probable velocity $v_m\left(=\sqrt{2RT_w}\right)$ nearly parallel to the oscillating lid, hitting the wall of $z = \mathcal{A}$, then being reflected and hitting the wall of $z = 0$, and finally returning to the point from which they left, should have traveled a distance of about $2\mathcal{A}$; say $v_m\delta t \approx 2\mathcal{A}$, where $\delta t$ is the traveling time. Therefore, if

$$\delta t = \frac{2n\pi}{\omega} \quad \text{or} \quad \frac{(2n-1)\pi}{\omega}, \quad n \in \mathbb{Z}^+, \tag{16}$$

molecules leaving and hitting the top lid should have the same (or opposite) phases.

When the velocity distribution functions for molecules leaving and coming back to the oscillating lid are in phase, the velocity $U_z$ near the oscillating lid reaches a maximum. Meanwhile, the average shear stress given by Eq. (6) is minimum since the molecules leaving and coming back to the lid have opposite $y$-component molecular velocities. The anti-resonance and resonance refer to the states where the shear stress exerted on the oscillating lid is minimum and maximum, respectively. Equation (16), together with Eq. (2), give the resonance number $\mathrm{St}_r$ and anti-resonance Strouhal number $\mathrm{St}_a$ as

$$\mathrm{St}_r \approx \frac{(2n-1)\pi}{2A_r}, \; n \in \mathbb{Z}^+ \tag{17}$$

and

$$\mathrm{St}_a \approx \frac{n\pi}{A_r}, \; n \in \mathbb{Z}^+. \tag{18}$$

Therefore, the dominant resonance Strouhal number $\mathrm{St}_r \approx \pi/2A_r$ and the anti-resonance Strouhal number $\mathrm{St}_a \approx \pi/A_r$ can be obtained by setting $n = 1$ in Eqs. (17) and (18). Additionally, Eqs. (17) and (18) suggest that the resonance and anti-resonance Strouhal numbers are independent of the depth ratio, which coincides with the observation from Fig. 8.

It should be noted that these analyses are for the free molecular flow. As the Knudsen number decreases, binary collisions of molecules become more frequent such that free transport of the gas molecules becomes less likely. Therefore, the real traveling time is larger than $2\mathcal{A}/v_m$, and the obtained $\mathrm{St}_a$ should be smaller than the theoretical value as given by Eq. (18). Furthermore, the flow inside the cavity requires sufficient kinetic energy to oscillate with the lid. As

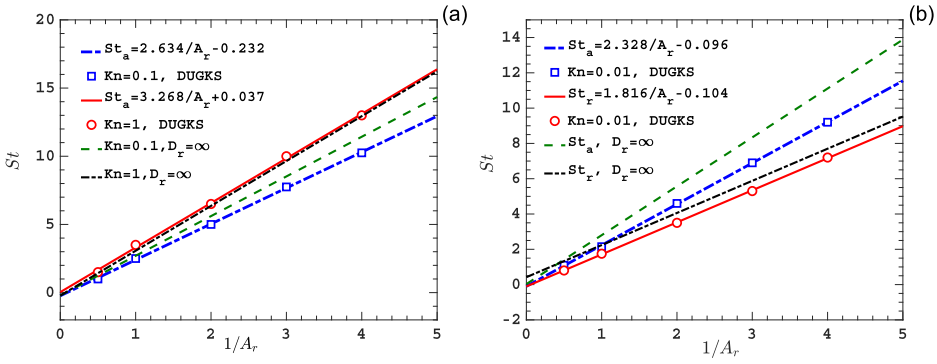


FIG. 9. The resonance (anti-resonance) Strouhal number $\mathrm{St}_r$ ($\mathrm{St}_a$), at which the average amplitude of shear stress at the oscillating lid is maximum (minimum), as a linear function of the inverse aspect ratio $1/\mathrm{A}_r$ for (a) Kn = 0.1 and 1 and (b) Kn = 0.01, when $D_r$ is set to be 0.5. The results of 2D in the limit of $D_r = \infty$ are also included for comparison.[20]

a consequence, resonance is only observed in the flows with small Knudsen numbers, instead of highly rarefied flows, see Fig. 7(a), where the oscillation quickly decays due to the large dissipation.

Depending on the inverse aspect ratio, the linear scaling laws for the anti-resonance Strouhal number with $D_r = 0.5$ are presented in Fig. 9(a) for Kn = 0.1 and 1 and Fig. 9(b) for Kn = 0.01. The same conclusions can be drawn for other values of $D_r$. We find that the fitting scaling laws for Kn = 1 are in good agreement with the theoretical value of $\pi/A_r$, while for Kn = 0.1 and 0.01, as analyzed above, the obtained value is smaller than the theoretical one, and the discrepancy becomes more pronounced as the Knudsen number reduces.

The scaling laws for anti-resonance in a 2D cavity,[20] i.e., $D_r = \infty$, are also included in Fig. 9. The relative errors between the 2D and 3D solutions are depicted in Fig. 10, which quantifies the effect of the 3D structure (i.e., the lateral walls) on the damping. We can see that the reduction in Kn leads to a larger relative difference for a given $A_r$. For example, the relative differences for Kn = 1, 0.1, and 0.01 are about 3%, 10%, and 18%, respectively. This is due to the fact that for a given dimension of the cavity, the lateral walls will produce a larger resistance force for the flow with a smaller Kn. In addition, we also notice that for all Kn, an increase in $A_r$ amplifies the relative difference between the 2D and 3D cavity results. This is because that with the given Kn and $D_r$, a larger $A_r$ results in a longer travel time $\delta t$, see Eq. (16), during which the transport molecules will be more likely affected by the lateral walls, thus leading to a greater impact of the lateral walls on the gas anti-resonance, as well as the gas resonance.

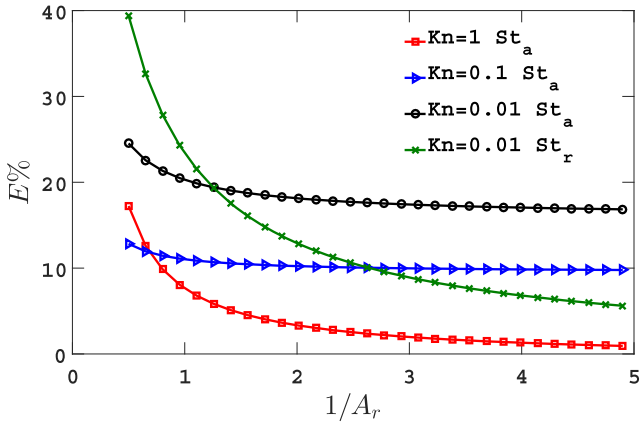


FIG. 10. The relative error $E\%$ for $\mathrm{St}_a$ or $\mathrm{St}_r$ between the 2D ($D_r = \infty$) and 3D ($D_r = 0.5$) simulations as a function of the inverse aspect ratio $1/A_r$. Here $E = 100\|\mathrm{St(3D)/St(2D)} - 1\|$.

The gas resonance appears at Kn = 0.01. The linear scaling law for the resonance Strouhal number with respect to the inverse aspect ratio with $D_r = 0.5$ is presented in Fig. 9(b), which is in reasonable agreement with the theoretical result given by Eq. (17). Similar to that for the anti-resonance, the relative difference between 2D and 3D cavities increases with $A_r$; see Fig. 10. In addition, for a relatively large $A_r$, the relative difference for $\mathrm{St}_r$ is even larger than that for $\mathrm{St}_a$, which indicates that the lateral walls produce a more significant effect on the gas resonance than on the gas anti-resonance. However, the situation is reversed when a small $A_r$ is applied.

## V. CONCLUSIONS

We have investigated the oscillatory rarefied gas flow in a 3D rectangular cavity. For small Knudsen number, as the depth ratio reduces, the damping force on the oscillating plane grows as expected. However, due to the strong rarefaction effect, this is reversed for a large Knudsen number with a low lid oscillation frequency, that is, the damping force in a 3D oscillatory cavity can even be smaller than that of the corresponding 2D cavity (i.e., the depth in the lateral direction of the cavity approaches infinity). Meanwhile, when the oscillation frequency is sufficiently high due to the gas anti-resonance, the damping force can increase again with reduction of the cavity depth for the highly rarefied flow.

One of the features of oscillatory flow is that the damping force exerted on the oscillating lid has local dips and peaks when the oscillation frequency changes. This is due to the anti-resonance and resonance of rarefied gas flows, respectively. It is found that the lateral walls on a 3D cavity suppress the formulation of gas resonance and anti-resonance. Depending on the inverse aspect ratio of the cavity, the linear scaling laws for the anti-resonance and resonance frequencies are obtained from the near hydrodynamic to highly rarefied flows, which are in reasonable agreement with the theoretical values. In addition, the obtained scaling laws are also compared with the solutions of 2D cases, which suggests that reducing the Knudsen number and increasing the aspect ratio of the cavity will enhance the 3D effect on formation of gas resonance and anti-resonance.

Our findings can help to improve design and operation of the micro-electro-mechanical devices. For example, the

resonant damping is identified as a major consideration for the device design and operation to prevent structural damage.

## ACKNOWLEDGMENTS

The authors would like to acknowledge Dr. Lei Wu for careful reading of the manuscript and critical comments. This work is financially supported by the UK's Engineering and Physical Sciences Research Council (EPSRC) under Grant Nos. EP/M021475/1 and EP/L00030X/1.

[1]C.-M. Ho and Y.-C. Tai, "Micro-electro-mechanical-systems (MEMS) and fluid flows," Annu. Rev. Fluid Mech. **30**, 579–612 (1998).
[2]A. Beskok and G. Karniadakis, *Microflows and Nanoflows: Fundamentals and Simulation*, Interdisciplinary Applied Mathematics (Springer, 2005).
[3]J. H. Park, P. Bahukudumbi, and A. Beskok, "Rarefaction effects on shear driven oscillatory gas flows: A direct simulation Monte Carlo study in the entire Knudsen regime," Phys. Fluids **16**, 317–330 (2004).
[4]A. Frangi, A. Frezzotti, and S. Lorenzani, "On the application of the BGK kinetic model to the analysis of gas-structure interactions in MEMS," Comput. Struct. **85**, 810–817 (2007).
[5]D. Kalempa and F. Sharipov, "Sound propagation through a rarefied gas confined between source and receptor at arbitrary Knudsen number and sound frequency," Phys. Fluids **21**, 103601 (2009).
[6]F. Sharipov, *Rarefied Gas Dynamics: Fundamentals for Research and Practice* (John Wiley & Sons, 2015).
[7]F. Sharipov and D. Kalempa, "Oscillatory Couette flow at arbitrary oscillation frequency over the whole range of the Knudsen number," Microfluid. Nanofluid. **4**, 363–374 (2008).
[8]J. H. Park and S. W. Baek, "Investigation of influence of thermal accommodation on oscillating micro-flow," Int. J. Heat Mass Transfer **47**, 1313–1323 (2004).
[9]S. Stefanov, P. Gospodinov, and C. Cercignani, "Monte Carlo simulation and Navier–Stokes finite difference calculation of unsteady-state rarefied gas flows," Phys. Fluids **10**, 289–300 (1998).
[10]N. G. Hadjiconstantinou, "Sound wave propagation in transition-regime micro-and nanochannels," Phys. Fluids **14**, 802–809 (2002).
[11]J. H. Park, S. W. Baek, S. J. Kang, and M. J. Yu, "Analysis of thermal slip in oscillating rarefied flow using DSMC," Numer. Heat Transfer, Part A **42**, 647–659 (2002).
[12]N. G. Hadjiconstantinou and A. L. Garcia, "Molecular simulations of sound wave propagation in simple gases," Phys. Fluids **13**, 1040–1046 (2001).
[13]D. R. Emerson, X.-J. Gu, S. K. Stefanov, S. Yuhong, and R. W. Barber, "Non-planar oscillatory shear flow: From the continuum to the free-molecular regime," Phys. Fluids **19**, 107105 (2007).
[14]D. Kalempa and F. Sharipov, "Sound propagation through a rarefied gas. Influence of the gas–surface interaction," Int. J. Heat Fluid Flow **38**, 190–199 (2012).
[15]T. Doi, "Numerical analysis of oscillatory Couette flow of a rarefied gas on the basis of the linearized Boltzmann equation," Vacuum **84**, 734–737 (2009).
[16]T. Tsuji and K. Aoki, "Gas motion in a microgap between a stationary plate and a plate oscillating in its normal direction," Microfluid. Nanofluid. **16**, 1033–1045 (2014).
[17]L. Wu, J. M. Reese, and Y. Zhang, "Oscillatory rarefied gas flow inside rectangular cavities," J. Fluid Mech. **748**, 350–367 (2014).
[18]D. R. Ladiges and J. E. Sader, "Variational method enabling simplified solutions to the linearized Boltzmann equation for oscillatory gas flows," Phys. Rev. Fluids **3**, 053401 (2018).
[19]L. Wu, "Sound propagation through a rarefied gas in rectangular channels," Phys. Rev. E **94**, 053110 (2016).
[20]P. Wang, L. Zhu, W. Su, L. Wu, and Y. Zhang, "Nonlinear oscillatory rarefied gas flow inside a rectangular cavity," Phys. Rev. E **97**, 043103 (2018).
[21]P. Wang, M. T. Ho, L. Wu, Z. Guo, and Y. Zhang, "A comparative study of discrete velocity methods for low-speed rarefied gas flows," Comput. Fluids **161**, 33–46 (2017).
[22]K. Xu, *Direct Modeling for Computational Fluid Dynamics: Construction and Application of Unified Gas-Kinetic Schemes* (World Scientific, 2015).
[23]W. Ye, X. Wang, W. Hemmert, D. Freeman, and J. White, "Air damping in laterally oscillating microresonators: A numerical and experimental study," J. Microelectromech. Syst. **12**, 557–566 (2003).
[24]P. L. Bhatnagar, E. P. Gross, and M. Krook, "A model for collision processes in gases. I. Small amplitude processes in charged and neutral one-component systems," Phys. Rev. **94**, 511 (1954).
[25]Z. Guo, K. Xu, and R. Wang, "Discrete unified gas kinetic scheme for all Knudsen number flows: Low-speed isothermal case," Phys. Rev. E **88**, 033305 (2013).
[26]Z. Guo, R. Wang, and K. Xu, "Discrete unified gas kinetic scheme for all Knudsen number flows. II. Thermal compressible case," Phys. Rev. E **91**, 033313 (2015).
[27]L. Wu, J. M. Reese, and Y. Zhang, "Solving the Boltzmann equation deterministically by the fast spectral method: Application to gas microflows," J. Fluid Mech. **746**, 53–84 (2014).
[28]W. Su, S. Lindsay, H. Liu, and L. Wu, "Comparative study of the discrete velocity and lattice Boltzmann methods for rarefied gas flows through irregular channels," Phys. Rev. E **96**, 023309 (2017).
[29]P. Wang, L. Zhu, Z. Guo, and K. Xu, "A comparative study of LBE and DUGKS methods for nearly incompressible flows," Commun. Comput. Phys. **17**, 657–681 (2015).
[30]Y. Bo, P. Wang, Z. Guo, and L.-P. Wang, "DUGKS simulations of three-dimensional Taylor–Green vortex flow and turbulent channel flow," Comput. Fluids **155**, 9–21 (2017).
[31]L. Zhu, S. Chen, and Z. Guo, "dugksFoam: An open source OpenFOAM solver for the Boltzmann model equation," Comput. Phys. Commun. **213**, 155–164 (2017).
[32]K. Xu and C. Liu, "A paradigm for modeling and computation of gas dynamics," Phys. Fluids **29**, 026101 (2017).
[33]L. Yang, C. Shu, J. Wu, and Y. Wang, "Numerical simulation of flows from free molecular regime to continuum regime by a DVM with streaming and collision processes," J. Comput. Phys. **306**, 291–310 (2016).